Canadian Geotechnical Journal
Revue canadienne de géotechnique

Shear bands in undrained plane strain compression of Norwegian quick clays

Journal:	*Canadian Geotechnical Journal*
Manuscript ID	cgj-2016-0443.R1
Manuscript Type:	Article
Date Submitted by the Author:	15-Feb-2017
Complete List of Authors:	Thakur, Vikas; Norwegian University of Science and Technology, Civil and Environmental Engineering Nordal, S.; Norwegian University of Science and Technology, Civil and Environmental Engineering Viggiani, Gioacchino; Universite Grenoble Alpes Charrier, Pascal; Universite Grenoble Alpes, L3S-R
Keyword:	plane strain testing, sensitive clay, strain localization, shear band

Shear bands in undrained plane strain compression of Norwegian quick clays

Vikas Thakur[1] and Steinar Nordal[2], Gioacchino Viggiani[3] and Pascal Charrier[4]

[1] Vikas.Thakur@ntnu.no , Norwegian University of Science and Technology, Norway, Phone: +47 41 29 57 17, Fax : +47 73 59 46 09

[2] Steinar.Nordal@ntnu.no, Norwegian University of Science and Technology (NTNU), Trondheim, Norway, Phone: +47 73 59 45 95, Fax : +47 73 59 46 09

[3] Cino.Viggiani@3sr-grenoble.fr, Univ. Grenoble Alpes, CNRS, Grenoble INP*, 3SR, F-38000 Grenoble, France

[4] Pascal.Charrier@3sr-grenoble.fr, Univ. Grenoble Alpes, CNRS, Grenoble INP*, 3SR, F-38000 Grenoble, France

* *Institute of Engineering Univ. Grenoble Alpes*

Shear bands in undrained plane strain compression of Norwegian quick clays

Abstract

This work presents results from plane-strain tests carried out at the Laboratoire 3SR Grenoble (France) on undisturbed samples of very sensitive Norwegian soft clay. Discussion of the results focuses in particular on failure mechanisms and observed zones of localized deformation. The tested clay is denoted as quick clay because it is known to liquefy completely upon remolding. Thus, careful handling was needed, and tailored procedures were developed to install the samples in the plane-strain device with minimum disturbance. The results show the development of excess pore water pressure during shear loading and a loss of shear strength after peak, which is a typical feature of sensitive soils. The sample is held between two glass plates, which allows visual tracking of the deformations. Digital Image Correlation analysis reveals a complex pattern of emerging shear bands until one or two bands dominate and provide a final failure mechanism. Two local pore water pressure transducers are attached to the sample boundary, showing differences in local pore water pressure. It is suggested that the measured excess pore water pressure depends on the distance from the transducers to the observed zones of concentrated shear strains.

Keywords: plane-strain testing, sensitive soft clay, strain localization, shear band, local pore water pressure measurements

Introduction

The sensitive or quick clays of Scandinavia are highly susceptible to liquefaction upon shear loading beyond peak strength (Bjerrum 1955; Janbu 1979; Karlsrud et al. 1985; Thakur and Degago 2012 & 2013; Thakur et al. 2014). This implies that even a modest triggering event may result in devastating landslides, such as the Rissa landslide (Gregersen 1981), the Kattmarka landslides (Nordal et al. 2009), the Byneset flow slide (Thakur et al. 2014). Determining the strength and stability of quick clay is therefore essential in Scandinavian geotechnical practice (*e.g.*, Bjerrum 1955; Janbu 1967; Karlsrud and Hernandez-Martinez 2013; Thakur et al. 2012&2014; Amundsen et al. 2015 & 2016). Unfortunately, stability evaluations using classical limit equilibrium methods exhibit shortcomings when applied to a strain-softening material (*e.g.*, Bernander 2000; Jostad and Andresen 2002; Jostad et al. 2006; Thakur 2007; Gylland et al. 2010; Jostad et al. 2014). The main shortcomings of *LE* methods are that peak strengths are considered along a potential shear surface; in reality, some soil along the shear surface may have experienced softening with loss of strength while peak shear strength has not been attained yet along other parts of the surface. Progressive failure mechanisms must be considered (*e.g.*, Andresen and Jostad 2007; Gylland et al. 2013; Thakur 2011; Grimstad and Jostad 2012). For Scandinavian quick clays, this involves modeling the strain-softening behavior, including progressive *propagation of* localized failure along a *shear band, which defines the slip surface. Most shear bands associated with slope failures develop under conditions very close to plane-strain. However, to the best of the authors' knowledge, no plane-strain tests have earlier been performed on quick clays, which have always been tested under more conventional triaxial conditions.*

This paper presents the results of a comprehensive laboratory testing program specifically designed to study the formation of shear bands in Norwegian quick clays under plane-strain conditions. Mechanisms for the formation and propagation of shear bands in Norwegian quick clays are studied using digital image correlation. Local pore water pressure (pwp) transducers are applied to see if localized deformation is accompanied by high pwp.

Background

General aspects of quick clays

During the last glaciation marine clays were formed in Scandinavia. When the ice disappeared, the land rose, and over the next 10.000 years sodium chloride was leached from the marine clays (Rosenqvist 1953). Large volume of the marine clay turned quick. In Norway, sensitive clays with remolded shear strength less than 0.5 kPa are defined as quick clays. Quick clays have a natural water content (w) higher than their liquid limit (w_L). Norwegian quick clays are brittle, and they have a plasticity index less than 10%. Thakur and Degago (2012, 2014), Thakur et al. (2013, 2014) have demonstrated that the remolded quick clays behave as a viscous fluid rather than a plastic solid.

Quick clays are typically classified in terms of sensitivity (S_t) which is the ratio of the intact shear strength (c_{ui}) to the corresponding remolded shear strength (c_{ur}) measured using the fall cone test at the same water content. Several classification systems have been proposed in the literature (Skempton and Northey 1952; Rosenqvist 1953; Norwegian Geotechnical Society (NGF) 1974). A synthesis of these classifications is presented in Table 1.

Undrained behavior of quick clays in triaxial compression

The quick clays of Scandinavia are soft and very sensitive to disturbance during sampling. This is illustrated in Fig. 1, which shows results from conventional undrained triaxial compression tests on Tiller quick clay using two different samplers with diameters of 160 and 54 mm. Despite careful sampling for both samplers, a higher peak strength is found when using the largest sampler. Sample disturbance similarly affects the pre-consolidation pressure obtained from the oedometer tests in Fig. 1. The 160 mm diameter high quality block sample shows a higher pre-consolidation pressure than the 54-mm diameter sample. Lacasse et al. (1985) and Lunne et al. (1997) suggested that sample disturbance causes partial microstructure collapse prior to loading. Quick clay samples exhibit strain softening when sheared in undrained conditions. Positive excess pwps are generated in undrained compression, which is consistent with the contractive behavior exhibited by quick clays when they are sheared in undrained conditions. This can be seen from the effective stress path presented in Fig. 1. Minimal sample disturbances result in a smaller pwp build up prior to failure and a larger pwp during strain softening. Interestingly, effective strength parameters, such as the cohesion (c) and friction angle (φ) at failure, are unique for the tested material regardless of the sample disturbance. Interpretation of triaxial test results of six different soft sensitive clays by Thakur et al. (2014) also shows that undrained soft sensitive clays exhibit strain softening due to shear-induced pwp and not due to cohesion and friction softening at strain level up to 10-20%. However, for a very large strain levels cohesion and friction softening may be observed.

Stability of quick clay slopes in undrained conditions

Rapid deviatoric loading beyond peak leads to pwp build up in quick clays. In a zone of concentrated shear deformation, increasing pwp will follow the increase of shear deformations. However, if failure does not occur immediately, this pwp will dissipate with time, accompanied by an increase in effective stresses and shear stress capacity in the band. *Two counterbalancing mechanisms may be seen: increasing shear deformations will increase the local pwp and local drainage reduces the pwp (Fig. 2).* The rate of loading and the material response in terms of stress changes with pwp inside and outside the shear band will control the failure process in the material (Bernander 2002; Thakur et al. 2005; Jostad et al. 2006; Thakur 2011; Gylland et al. 2012; Jostad et al. 2014). *In the current paper this behavior is studied experimentally using plane-strain tests with appropriate loading rates under globally undrained conditions.*

Literature review on plane-strain testing of fine-grained materials

In recent decades, many experimental studies of strain localization have been performed by different research groups for a variety of geomaterials such as rock, sandstones, sand, stiff clays and soft clay. Finno and Rhee (1992), Viggiani et al. (1994), Lizcano et al. (1997), Viggiani et al. (2001), Chen (2004), Yuan et al. (2013), and Gylland et al. (2014) confirms that shear banding may take place in both contractive and dilative clay specimens, but for the latter, the onset of localization is delayed until cavitation take place in the pore fluid. It clear from the available literatures that soft clays have taken some attention but not as much as that of stiff clays. The formation and orientation of shear bands in sand is comprehensively discussed by Desrues and Viggiani (2004) and the several reference cited therein.

In the literature only few experimental studies related to the plane strain compression testing in soft clays have been reported; for instance Topolnicki et al. (1990), Finno and Rhee (1992), Lizcano et al (1997), Cheng (2004) and Yuan et al. (2013). Most of these studies have focused on investigating shear band thickness, local dilatancy angle, void ratio in the vicinity of the shear band, and orientation of the shear band. A recent study by Yuan et al. (2013) on two different medium plastic silty clays measures dilatancy in shear bands and locally lower pwps in the vicinity of these bands than further away.

Viggiani et al. (1994) have brought focus on shear band analysis for stiff clays tested in an undrained plane strain compression apparatus. Similarly, Marello (2005) also provided comprehensive information on propagation and formation of shear bands in stiff clays using a plane strain compression apparatus. False Relief stereo photogrammetry technique was used for the image correlation. Both the studies report local changes in the pwp within the specimen at the onset of localization. The pwp later smoothed by local drainage within the clay specimen.

Cheng (2004) studies the formation and the propagation of cracks in organic clays. Three different rates have applied; 0.5mm/hr, 1mm/hr and 5mm/hr. The tests resulted in the cracks forming near to the top plate. The pwp measurements were made at the center of the ends of specimens. Cheng (2004) concludes that soft organic clays exhibits strong discontinuity, in a form of cracks or just as interfaces, instead of shear bands. Gylland et al. (2014) have reported an experimental investigation on formation and propagation of shear bands in a Norwegian sensitive clay using a modified triaxial cell allowing for shear band formation. They studied the effect of varying the displacement rate on the onset of strain localization and on the softening response of the tested material. A reduced shear band thickness and a shear band inclination approaching 45^{o} were obtained for increasing displacement rates.

Laboratory experiments

Material tested: Tiller quick clay

The quick clay chosen for this study was sampled from Tiller, located approximately 10 km southeast of the city of Trondheim in Norway. The area is covered by a quick clay deposit approximately 10 m in depth overlain by a silty, low-sensitivity marine clay. The samples for this study were carefully recovered from two different bore locations at depths between 6 and 10 m using a 95 mm piston sampler with a steel cylinder. Routine characterization and index tests were carried out, the results of which are summarized in Table 2. It should be emphasized, however, that the Tiller quick clay deposit covers a large area; thus, certain variations in soil properties (both laterally and with depth) should be expected, as shown in the table. The odometer tests performed by Gylland et al. (2013) and Amundsen et al. (2017) suggest that the overconsolidation ratio of the quick clay deposit varies between 1.3-1.6, and the effective earth pressure coefficient at rest (K_o') for the deposit is 0.6. A low-sensitivity soft clay specimen (referred to as T6) was also tested in the test study. This sample was taken from the same area, but the sensitivity and remolded shear strength of the sample were 20 and 1.5 kPa, respectively. By definition, this is not a quick clay, although it is still sensitive.

The plane-strain apparatus

The plane-strain apparatus at Laboratoire 3SR was originally developed in Grenoble by Desrues (1984) and later modified by Hammad (1991). The design of such a device shares its underlying concept with those developed by Vardoulakis and Goldscheider (1981) and Drescher et al. (1990) in that the plane-strain apparatus is specifically conceived to allow free shear-band formation in a soil specimen. The top plate is free to slide horizontally (but not to rotate) in the plane of deformation. The lower and upper loading plates house porous stones connected to drainage lines. A large cell, filled with silicone oil, surrounds the specimen. The cell sustains up to 2 MPa. Two opposing pairs of 50-mm-thick glass plates windows support the sample laterally and provide plane strain conditions. Strain-controlled axial loading is applied through a screw jack that rested atop the device. An LVDT measures the vertical displacement, while the axial load is measured by an internal load cell at the top. Cell pressure is supplied by a compressor and monitored by a pressure transducer, while a self-compensating mercury control is used to apply a backpressure to the cell oil and pore water. The output signals of all transducers are conditioned by a process interface unit, which was linked to a microcomputer controlling all operations. (Desrues and Viggiani, 2004)

A 34-mm-thick prismatic specimen surrounded by a latex membrane is mounted between two rigid glass plates, inducing the plane-strain conditions. In this study, the initial height and width of the specimen (in the plane of deformation) are 120 mm and 60 mm, respectively. The sidewalls allow photographs to be taken of the in-plane deformation of a specimen during the test. Glass surfaces in contact with the specimen are lubricated with silicone grease to minimize friction. The plane strain apparatus used is shown in Fig. 3. Further details of the plane strain apparatus and the testing procedure can be found in Desrues and Viggiani (2004) and the references cited therein.

Specimen preparation and instrumentation

Large specimens (120 mm x 60 mm x 34 mm) were carefully cut from the 95-mm diameter samples. Although the standard sampler size in Norway is 54 mm, a 95 mm sampler was used in this study to obtain a higher sample quality, motivated by Lacasse et al. (1985) and Lunne et al. (2007). A block sampler was not available. To avoid disturbing the sensitive specimens, a special arrangement had to be developed to mount the quick clay specimen in the biaxial plane-strain apparatus. A splitting- and sliding-type stainless-steel mold was prepared to place the specimen into a stretched latex membrane. The working principle of the mold is: the inner mold holds the specimen while the outer shell stretches the membrane. The advantage of the arrangement is that it allows us to place a specimen into the membrane with minimum disturbance. This process is explained using a set of photographs in Fig. 4.

Once the specimen is placed inside the membranes, two temporary supports are attached to it. These additional supports were needed to transfer loads (such as self-weights and external forces) directly from the top plate to the bottom plate without damaging the quick clay sample while fixing the top plates, connecting the drainage lines, and inserting the pwp transducers.

These supports were removed only after the specimen was completely mounted in the apparatus. O-rings were used to seal the contact between membrane and the (top and bottom) plates. Fig. 4 also shows these two vertical supports that connect the top and bottom plates. A typical final set up of the specimen is presented in Fig. 5.

The present study attempts to address pwp induced softening in shear bands. In an attempt to measure this miniature pwp transduces are used to measure local pwp, Fig 5. The miniature pwp probes were calibrated so that small fluctuation in pwp could be captured. See Hight (1982) for details. Unfortunately, pwps could not in addition and simultaneously be measured in the filter stones at the sample top and bottom due to equipment restrictions. The two miniature probes were mounted onto the surface of the specimen in two different layouts: 1) on left or right side of the sample at mid-height, 60 mm from the top of the specimen (LP or RP); and 2) both on the same side of the specimen, one at mid-height (CP) and the other at one-quarter of the height from the top (TP) or bottom (BP). The top probe (TP) is thus located 30 mm from the top, and the bottom probe (BP) is located 30 mm from the bottom. The location of the probes were chosen based on assumed positions of possible shear bands. The intention was to see if pwp would increase more in the probe closer to an emerging and propagating shear band. The probes were carefully placed on the surface of the specimen to avoid disturbing the contact zone. As shown in Fig 5, two O-rings were used on each rubber socket to seal the contact between the membrane and the probes. See Hight (1982) for details. Utter care was taken to bring the pwp probes in touch with the surface specimen and keep them at that location. As can be seen in Fig. 5, a mesh was printed on the membrane before mounting. A series of 10-megapixel resolution digital photographs were taken at during the compression tests.

Test program

A series of plane strain tests were conducted, each of which included plane strain consolidation at a selected effective mean stress followed by undrained compression, Table 3. The consolidation stress was applied in the x-z direction, Fig. 5., and chosen at the level of the expected in situ horizontal effective stress, at 60 – 70kPa. Experience has shown that consolidation to higher effective stresses may destroy a transported quick clay sample. A small back pressure of 10 -15 kPa was used. The tests were run under displacement control, and two different rates of axial shortening were chosen: 0.06 mm/min and 0.006 mm/min. Note that the former value corresponds to the rate typically used in standard undrained triaxial tests on quick clay. The globally undrained condition was imposed by simply closing the drainage valves. Table 3 gives a short summary of the experimental program.

During the consolidation phase, two-way vertical drainage through the top and bottom was imposed. Note that during consolidation, plane strain conditions need to be maintained. There is a danger that the thickness of the specimen (in the direction orthogonal to the sidewalls) can reduce so a gap could form between the specimen and the sidewalls. The consolidation stress had to be carefully selected and applied in order to maintain full contact between the sample and the glass walls. As far as it could be seen, this was satisfied for all test reported herein.

Shear stress and deformation pattern of quick clays

Shear stress (t) and deformation patterns recorded for the tests are presented Fig. 7. Here, shear stress (t) is $(\sigma_z{}' - \sigma_x{}')/2$ where σ are the effective stresses; the subscripts z and x stand for the axial and horizontal direction in the plane of deformation. The peak shear stress (t_p) varied from 20 -30 kPa for quick clay samples and about 60 kPa for the non-quick clay sample (the T6 test). The failure axial strain (ε_p) varied from 2- 8%. As expected, we observe strain softening after a peak except for the T1 test, which show low peak strength and thus is believed to be disturbed. The peak shear stress is for the other tests reduced by 30-50% when they were sheared to 10 – 15% nominal axial strain level (vertical deformation of the sample top divided by the initial sample height). The normalized peak shear stress (t_p/σ_{zo}') for the quick clay specimens were 0.25 – 0.35. Here, σ_{zo}' is the in-situ effective vertical stress, while T6 show a surprisingly high value of 0,5. The obtained range of t_p/σ_{vo} is in line with the data reported by Gylland et al. (2014) for the quick clay.

The results show that the quick clays tested in plane-strain compression exhibited somehow non-smooth stress-strain patterns. On contrary to this, Fig. 1 suggests that quick clays exhibit smoother stress-strain response when subjected to undrained triaxial loading. Such distinction in the stress-strain response between triaxial and the plane strain test results may be attributed to the imposed boundary conditions (stick slip against the glass plates) and / or the emergence and propagation of shear bands during the tests. Readers are referred to Scavia et al. (1997), Charrier et al. (2001), Viggiani et al. (2001), Marello et al. (2003), and Desrues and Viggiani (2004) for more information in this regard.

The emergence and propagation of shear bands during the undrained shearing phase were recorded using a continuous movie for tests T1, T3, and T4 and by a series of 10-megapixel resolution images taken at different nominal axial strain levels during tests T2, T5, and T6. Image analyses were carried out using the Davis V8.0 (2015) digital image correlation (DIC) tool.

Digital Image Correlation (DIC) is essentially a mathematical tool for assessing the spatial transformation (including translations and distortions) between two digital images. In practice, DIC is implemented as a computer program that allows regions of a photographed object to be tracked automatically from one digital image to the next, from which displacements can be deduced. From the measured displacement field, a strain field can be derived, which is based on the gradients of the derived displacements and a continuum assumption. A number of textbooks and papers describe the technique in detail, see for example Hall (2012) and the many references given therein. In this study, DIC was carried out carried out using the commercial software Davis V8.0 (2015).

The DIC analyses were carried out for the T2, T5, and T6 tests. The results in terms of total and incremental shear strain distributions are presented in Figs. 7, 8, and 9, respectively. The incremental strain distributions were obtained for two consecutive images, while the total strain distributions result from comparing a state with its initial state. It must be noted that the image correlation for two images over long intervals may obscure certain important information; therefore, the selected intervals should be rather small for accurately capturing deformation behavior. In the later part of this paper, the onset, formation and propagation of bands during the tests were investigated using a term denoted the pwp non-uniformity (Δp_w). Here, Δp_w refers to a difference between the pwp readings from the two probes on a sample.

T2 test

The shear stress (t) versus nominal axial strain (ε) is presented in Fig. 7 along with the corresponding maximum deviatoric strain distribution resulting from the image correlations for images taken from the start (P0) through the end of the test (P8). Pore water pressure non-uniformities, Fig. 7(b) is discussed later. The total shear strain accumulated inside the sample was measured and obtained using the DIC analysis of the images (P1 to P8) with respect to P0, as shown in Fig. 7(c). The shear strain distribution between two consecutive images is shown in Fig. 7(d).

The incremental shear strain distribution corresponding to the numbered points P0–P1 in the figure shows a slightly non-homogenous deformation in the test specimen where the incremental strains are concentrated in the upper part of the specimen. This result indicates that localization initiates before peak (in the hardening regime). The P1–P2 result indicates an emergence of a shear band at the upper left corner of the specimen. The P3–P4 result shows a fully developed curved shear band emerging from the upper left to the middle right of the sample. This observation is associated with a distinct drop in the shear stress between P3 and P4. In addition, the P3–P4 result also shows the emergence of a new shear band from the upper right edge of the specimen. The P4–P5 and P5–P6 results show completely new shear bands from the upper right edges of the specimen progressing towards the lower left ends. However, at this stage, the progression of the previously observed shear bands at P3–P4 appears to be halted, which is a peculiar behavior at this stage because the shear stress is gradually decreasing. Finally, the P7–P8 result shows that cross-shaped but non-symmetrical shear bands are formed by the end of the test.

The DIC results indicate that the shear band formation process in the quick clay was progressive, non-symmetric, and complex. The total and incremental shear strain distributions suggest that the propagation of the shear bands was smooth and gradual, and the shear bands were non-unique and alter throughout the test (see Fig. 7). This observation also indicates that certain parts of the shear bands must be subjected to more strain softening than others. The failure process continued until a kinematic mechanism was formed, dividing the sample into several shear bands and non-localized zones. The shear strain inside the localized zones (e.g.

~ 30% for P0-P8) are in order of three times the globally applied nominal strain (~ 10% at P8). The 10% nominal axial strain corresponds to 12 mm deformation. Accordingly, the thickness of localized shear band could be 36 mm. An accurate thickness of shear bands is difficult to measure for the membrane wrapped specimen. At the end of the test, the orientation of the shear bands varied from 45-50^{o} from the horizontal planes as they were curved.

T5 test

The P2–P3 result shows a gradual growth of localized shear zones. The P3–P4 result shows a distinct shear band emerging from the upper left edge of the specimen prior to the peak. The P4–P5 and P5–P6 results vaguely indicate a completely developed shear band that amplifies in P6-P7 at a 53° inclination from the horizontal planes. In the post-peak region, a new shear band emerges upward from the lower left of the specimen and proceeds toward the center (the P6-P7). Finally, the P7–P8 reveals a nearly cross-shaped shear band inside the specimen, but the majority of the localized strains were concentrated inside the original shear band already observed at the peak, whereas the other shear band located in the lower left to the upper right seems to not grow further. Similar to T2 test, at the end of the test, the maximum shear strain inside the localized zones (e.g. ~ 30% for P0-P8) is order of again three times the globally applied nominal strain (~ 12% at P8). However, at the peak shear stress (P4-P5) the thickness of the shear band found to be around 4-5 mm only. The thickness of the shear bands or the localized zones towards the end seems to be much larger. The DIC analysis shows that the new shear bands emerged and fluctuated throughout the test.

T6 test

Fig. 9 shows a rather diffuse deformation mode before reaching peak for the T6 test, unlike the other two tests. It must be noted that the T6 test was carried out on less-sensitive clay. The P1–P2, P2–P3, and P0–P3 results reveal localized zones at the peak from the upper left and right edges of the test specimens. At the peak, the P3–P4 result shows that a partially developed shear band emerges from the upper part of the specimen. Cross-shaped shear bands (P4–P5) simultaneously develop around an 8–9% nominal axial strain and continue to grow until the end of the test. Finally, the P5–P6, P6–P7, and P7–P8 results show a fully developed, nearly symmetric cross-shear band. The DIC result for the T6 test indicate several thinner shear bands forming the final kinematic failure mechanism. The shear bands tend to initiate in the upper portion of the sample but moves downwards and steepens towards the end of the test.

The T6 test resulted in an almost symmetric failure mode. The T2 and T5 tests show that the shear bands were initiated locally and gradually grew until the quick clay specimens were split into several localized zones. The thickness of shear bands varied throughout the test. Thakur and Degago (2012, 2013), Thakur et al. (2013, 2014) suggests that the collapse behavior of sensitive clays with a remolded shear strength over 1 kPa is not as metastable as that of quick clays. In other words, sensitive clays having remolded shear strength over 1 kPa (As T6) is more or less a solid material and therefore they don't flow, whereas quick clays flow when they are remolded. This can explain why the *T6* test results are more similar to failure patterns seen in less sensitive clays.

Discussion on local pore water pressure measurements

The effective stress paths obtained by using pore water pressures (pwp) measured at the two probe locations are presented in Fig. 10. The local pwp measured by the two probes make the two stress paths for each test different. In addition, the minor differences in the residual pwp at the end of the consolidation stage caused a different initial effective stresses at the probe locations. The local effective stress paths for the tests are plotted in terms of *s'*- *t* plots. In this figure, *s'* represents the mean effective stresses ($(\sigma_z{}' + \sigma_x{}')/2$), and σ' are the effective stresses; the subscripts *z* and *x* stand for the axial and horizontal direction in the plane of deformation shown in Fig. 5, respectively. The positive pwp generated during the tests confirms that the quick clays exhibit contractive behavior during undrained shearing. Some of the irregular shape of the initial part of the effective stress paths in some of the tests could be related to a stick–slip friction against the glass walls. A stress path inclining 1:1 in this plot would result if a test was drained. We observe tendencies that parts of the stress paths has such an inclination. This may suggest that there is some air in the system and that we do not have ideal undrained conditions. Effective stress paths are seen generally not to end on the Mohr Coulomb failure line in the figure. This might be simply caused by local pwp variations due to localized deformations. We are unable to measure the pwp in the shear band and do not have the average pwp to go with the average total stresses s and t.

The pwp measurements from the two different pwp probes were quite different. A minor part of the difference in pwps was caused by the different residual pwp at the end of the consolidation stage. The residual pwp is largest at the center of the sample. To focus on differences in the development of the pwp towards failure, the pwp data shown in Figs 7, 8 and 9 are reset to zero at the start of the shearing stage which corresponds to nominal axial strain (ε) = 0%, while Fig 11 show the actual measured values.

We observe that the excess pwp are much smaller in the tests run at 0.006 mm/min (T5 and T6) compared to the values found for 0.06 mm/min (T1 – T4). The opposite would have been expected based on previous quick clay experience: Rapid tests normally show higher peak strength and lower pore water pressures. Slow tests show less peak strength, earlier collapse and higher pore water pressures. At the beginning, test T5 and T6 shows a tendency to build higher excess pwp however with increasing deformation the pwp is much small. The current results indicate that there could some air in the system and that the condition of a globally fully undrained condition is not fully present. Dissipation into filter stones etc. will be more pronounced when time is allowed for it. This T5 and T6 show rather low pore water pressures. The stress paths in Fig 10 is hence "more drained" than the others. The results of all the tests at 0.06 mm/min indicate that the pwp response does not show many peaks or sudden drops during the shearing. However, the tests at 0.006 mm/min provide a more complex variation in the pwp. pwp

Pore water pressure non-uniformities

The direct measurement of pwp inside the shear bands can be a challenging task due to difficulties in predicting the location of the bands prior to the test. However, measurements near the shear bands may also provide significant information related to the onset of localization and the local drainage situation. A variation in pwp between the two probes should occur upon the emergence of a shear band close to one of the probes. Such behavior has been observed for the stiff clays Viggiani et al. (1994). Yaun et al. (2013) presented such results for dilating Shanghai silty clays.

The *(b)* plots in Figs. 7, 8, and 9 show the normalized pwp non-uniformities ($|\Delta p_w|/\sigma_{xo}'$) for the T2, T5, and T6 tests, respectively. The $|\Delta p_w|/\sigma_{xo}'$ is the difference in the measurements recorded by the two probes on one sample, and the emergence of shear bands and the variation in Δp_w are interrelated, as shown in these figures. A decrease in the $|\Delta p_w|/\sigma_{xo}'$ was often observed when the shear bands were fully developed. However, the $|\Delta p_w|/\sigma_{xo}'$ increased when the shear bands propagated or grew progressively. The correlation between the DIC results and the $|\Delta p_w|/\sigma_{xo}'$ for the T2 test shows that the emergence of the shear band and the first peak in the $|\Delta p_w|/\sigma_{xo}'$ were observed at a 4% nominal axial strain. At this stage, the DIC results for P1-P2 result indicates the emergence of a shear band at the upper left corner of the specimen.

Similarly, the emergence of shear bands and peaks in the $|\Delta p_w|/\sigma_{xo}'$ were recorded at 2% and 6.4% nominal axial strain, respectively, for the T5 test. As mentioned earlier, a distinct shear band appeared at 2% nominal axial strain, which led to the growth of a distinct shear band from the upper left corner of the specimen. A sudden drop in $|\Delta p_w|/\sigma_{xo}'$ as well as in the shear stress was registered. A reduction in $|\Delta p_w|/\sigma_{xo}'$ beyond 6.4% nominal axial strain could be again related to reduction in the peak shear stress. The DIC results also confirms that at these nominal axial strains. Peaks in the $|\Delta p_w|/\sigma_{xo}'$ were noted at 1.5%, 5.5%, 7.5%, and 11.5% axial deformation for the T6 test associated with the initiation and propagation of shear bands inside the specimen. Interestingly, these peaks were difficult to note in the Fig.9(d) plot for the T6 test.

The fluctuations in shear bands observed resulted in multiple peaks in $|\Delta p_w|/\sigma_{xo}'$ throughout the test. The peaks in pwp non-uniformity observed for the T2 test and for Shanghai silty clay, as reported by Yuan et al. (2013), are compared in Fig. 12. Clearly, the trends are remarkably identical, i.e., the $|\Delta p_w|/\sigma_{xo}'$ increased until the onset of localization (O) and there were insignificant variations in the $|\Delta p_w|/\sigma_{xo}'$ until the formation of the primary shear band was completed (B). One shall expect $|\Delta p_w|/\sigma_{xo}' = 0$ for an homogenously deforming specimen, however the measured data suggests that soft clay specimen may be subjected to non-uniform deformation prior to the onset of localization e.g. $|\Delta p_w|/\sigma_{xo}' > 0$.

Unfortunately, pwp variations between the two probes may also be caused by other effects. In spite of careful calibration measurements errors can not be totally excluded. Further, variations in pwp during testing may be due to equalization of residual pwps remaining after an unfinished consolidation phase, friction between the specimen and the glass wall, or friction between the top/bottom plate and specimen, or non-homogenities in the specimen itself. It should be noted that a sudden increase or decrease in the $|\Delta p_w|/\sigma_{xo}'$ was not observed in any of the tests performed in this study, in contrast to the observations by Viggiani et al. (1994) for still clays. The present study illustrates a complex interaction between generations of pwp in shear bands and shear band formation. Non-smooth stress deformation pattern and irregular excess pwp are associated with the formation and propagation of shear bands in quick clays. However, in absence of DIC results the onset of shear bands were difficult to register for quick clays based on the $|\Delta p_w|/\sigma_{xo}'$ values alone.

Conclusions

This study presents results related to the behavior of quick clays under plane-strain conditions. Localized deformations are seen to occur in fluctuating shear bands before a final failure mechanism is formed. The results from the DIC revealed that the process by which shear bands are formed in the quick clays is quite complex. Formation of the shear bands was progressive, non-symmetric, and seemingly random. The shear bands were observed to fluctuate throughout the tests. The accumulated strain inside shear bands were as high as three to four times the applied nominal axial strains. The total and incremental shear strain distributions shows that that certain parts of the shear bands are subjected to more strain softening than others. The failure process continued until a kinematic mechanism is formed, dividing the sample into several shear bands and non-localized zones. The pwp measurements taken at two different locations on the surface of the quick clay samples show that shear banding involves significant variations in the buildup of pwps within the sample followed by local drainage of pore water within the sample. The local effective stress paths suggest that unloading was prevented in the neighboring soil material due to the flux of pore water to this soil volume from the shear bands. If the observation is correct, this implies that failure is less brittle than it otherwise might have been. The pwp measurements show that the differences in locally measured pwps may indicate the onset of localization and gradual progression of the shear bands inside the tested samples. The differences in locally measured pwps are rather modest in this study on quick clays and are not as abrupt and large as those for the stiff clays reported in the literature. This may be due to a low stress level in the present study and some sample disturbance, which is hard to avoid for quick clays. A decrease in the pwp non-uniformities was often observed when the shear bands were fully developed. However, the pwp non-uniformities increased when the shear bands propagated or grew progressively. The study confirms a complex process in the formation and propagation of shear bands in quick clays.

Acknowledgements

Dr. H. P. Jostad from the Norwegian Geotechnical Institute is gratefully acknowledged for his kind support. Authors are thankful to Dr. J. Desrues from Laboratoire 3SR for timely discussions. The Geotechnical Group at NTNU, Norway, is acknowledged for their help and technical assistance. The author is thankful to the International Centre for Geohazards NFR-CoE-ICG, Norway, for providing financial support to this study. Dr. Samson Degago from the

Norwegian Public Roads Administration is gratefully acknowledged for the manuscript editing and invaluable feedback. Ms Helene Amundsen is acknowledged for providing the triaxial and odometer tests results.

References

1. Amundsen, H. A., Thakur, V., and A. Emdal. 2016. Sample disturbance in block samples of low plastic soft clays. 6th International Conference on Geotechnical and Geophysical Site Characterization, Queensland, Australia (in press).
2. Amundsen, H. A., Thakur, V., and Emdal A. 2015. Comparison of Two Sample Quality Assessment Methods Applied to Oedometer Test Results. *In* Proc. Of the 6th Int. Symp. On Deform. Charact. Of Geomat., Vol. 6, pp. 923-930.
3. Amundsen, H. A., Jønland J, Emdal A. and Thakur V 2017. An attempt to monitor pwp changes in a block sample during and after sampling. *Geotechnique Letters* (under review).
4. Bernander, S. 2000, Downhill progressive failure in long natural slopes, Licentiate Thesis, Luleå University.
5. Bjerrum, L. 1955. Stability of natural slopes in quick clays. Geotechnique **5**(1):101-119.
6. Charrier. P., Desrues, J., Lenti, L., and Viggiani, G. 2001. Experimental observation of strain localization in plane strain compression of Beaucaire marl. Internal report to IGS, Stuttgart, Germany.
7. Chehab, G., Seo, Y., and Kim, Y. 2007. Viscoelastoplastic Damage Characterization of Asphalt–Aggregate Mixtures Using Digital Image Correlation. International Journal of Geomechanics, **7**(1): 111–118.
8. Cheng, X. 2004. Localization in Dutch dune sand and organic clay. PhD thesis, TU Delft, The Netherlands.
9. Davis .2015. Davis LaVision. Version 8. www.lavision.de
10. Desrues J., and Duthilleul B. 1984. Mesure du champ de déformation d'un objet plan par la méthode stéréophotogrammétrique de faux relief. Journal de Mécanique Théorique et Appliquée, **3**(1): 79-103.
11. Desrues J.1984. La localisation de la deformation dans les mat !eriaux granulaires. Th"ese de 22eomechanic Science, USMG and INPG, Grenoble, France.
12. Desrues J.1990. Shear band initiation in granular materials: experimentation and theory. Geomaterials Constitutive Equations and Modelling. Elsevier: Amsterdam: 283–310.
13. Desrues, J., and Viggiani, G. 2004. Strain localization in sand: an overview of the experimental results obtained in Grenoble using stereophotogrammetry. International Journal of Numerical and Analytical Methods in Geomechanics, **28**(4): 279-321.
14. Finno, R. J., and Rhee, Y. 1992. "Kinematically unconstrained compression of soft clay." Proceedings of a specialty Conference on Stability and Performance of Slopes and Embankments, ASCE, Berkeley, 2, pp.142-157.
15. Gregersen, O. 1981. The quick clay landslide in Rissa, Norway. Proc. 10th Int. conf. on oil Mechanics and Foundation Engineering, Stockholm, 3, pp. 421-426.

16. Grimstad, G., and Jostad, H.P. 2012. Stability analyses of quick clay using FEM and an anisotropic strain softening model with internal length scale. Nordic Geotechnical Meeting, Copenhagen, pp. 675-680.
17. Grimstad, G., Thakur, V., and Nordal, S. 2005. Experimental investigation of formation and propagation of shear zone in Norwegian quick clay. 11th International Conference on Field Trips to Landslides, Trondheim, Norway, pp. 137-141.
18. Gylland, A., Jostad H.P., and Nordal S. 2013. Experimental study of strain localization in sensitive clays. Acta geotechnica, **9**(2): 227-240.
19. Gylland, AS, Long, M., Emdal, A., Sandven, R. 2013 Characterisation and engineering properties of Tiller clay. Engineering Geology. vol. 164, pp. 86-100.
20. Gylland, A., Sayd, M., Jostad, H. P., and Bernander, S. 2010. Investigation of soil property sensitivity in progressive failure. Proc. Of the 7th European Conf. on Num. Meth. In Geotech. Eng. In T. Benz and S. Nordal (Eds.), Trondheim, Norway, pp. 515-520.
21. Hight D.W. (1982) - A simple piezometer probe for routine measurement of pwp in triaxial tests on saturated soils. Géotechnique, Vol. 32, No. 4, 396-401.
22. Hall S.A. (2012) - Digital Image Correlation in Experimental Geomechanics. In: Advanced experimental techniques in geomechanics, G. Viggiani, S.A. Hall and E. Romero Eds., 69-102.
23. Hammad, W. 1991. Modélisation non linéaire et étude expérimentale des bandes de cisaillement dans les sables. PhD Thesis, University Josef Fourier, Grenoble, France.
24. Han C, Vardoulakis I.1991. Plane strain compression experiments on water-saturated fine-grained sand. Geotechnique, **41**(1):49–78.
25. Han C. 1991. Localization of deformation in sand. Ph.D. Dissertation, University of Minnesota, Minneapolis.
26. Han, C. and Vardoulakis, I. G. 1991 Plane-Strain Compression Experiments on Water-Saturated Fine-Grained Sand, Géotechnique, **41**(1): 49-78.
27. Harris WW, Viggiani G, Mooney MA, Finno RJ.1995. Use of stereophotogrammetry to analyze the development of shear bands in sand. Geotechnical Testing Journal, ASTM, 18(4):405–420.
28. Janbu, N.1979. Failure mechanism in quick clay. Nordic Geotechnical Meeting, Helsingfors.
29. Jostad, H. P., and Andresen, L. 2002. Bearing capacity Analysis of Anisotropic and Strain-Softening Clay." Numerical Models in Geomechanics Proceedings of the 8th International Symposium NUMOG VIII, Rome, Italy, pp. 469–474.
30. Jostad, H. P., Andresen, L., and Thakur, V. 2006. Calculation of shear band thicknesses in sensitive clays. Proceedings of the 6th European conference for Numerical Methods in Geotechnical Engineering, Austria, pp. 27-32.
31. Jostad, H.P., Fornes, P., and Thakur, V. 2014. Effect of strain-softening in design of fills in gently inclined areas with soft sensitive clays. First international workshop on landslide in sensitive clays. Advances in Natural and Technological Hazards Research 36, Chapter: 24, Publisher: Springer, pp. 305-316.
32. Karlsrud, K. and Hernandez-Martinez, F.G. 2013. Strength and deformation properties of Norwegian clays from laboratory tests on high quality block samples. Canadian Geotechnical Journal, **50**(12):1273-1293.
33. Karlsrud, K., Aas, G., and Gregersen, O .1985. Can we predict landslide hazards in soft sensitive clays? Summary of Norwegian practice and experience. NGI Publication 158.
34. Lenoir N., Bornert M., Desrues J., Bésuelle P., and Viggiani G. 2007. Volumetric digital image correlation applied to X-ray microtomography images from triaxial

compression tests on argillaceous rocks. International Journal for Experimental Mechanics, **43**(3) : 193-205.
35. Lizcano, A., Vardoulakis, I., and Goldscheider, M. 1997. Biaxial tests on normally anisotropically consolidated kaolin clay. Inelastic Deformation and progressive failure in 24eomechanics, Pergamon, UK, pp. 223-227.
36. Lu, X. B., Wang, S.Y., and Peng, C. 2004. On the evaluation of simple shear in saturated soils." International Journal of Numerical and Analytical Methods in Geomechanics, **28**(3), 269-278.
37. Marello, S. 2005. Experimental study of shear bands in fine grained soils. 11th International conference on computer methods and advances in geomechaincs, IACMAG, Torino, Italy, 2, pp. 119-126.
38. Marello, S., Lenoir, N., Viggiani, G., Bésuelle, P., Desrues, J., and Di Michiel M., (2003). Shear banding in plane strain compression of Beaucaire Marl studied through post-mortem X-ray micro tomography. Proc. Of the International Workshop on X-ray CT for Geomaterials, Soils, Concrete, Rocks, GeoX 2003, Kumamoto, Japan, Otani, J. and Obara Y. Eds., Balkema, pp. 39-146.
39. Mokni M, Desrues J. 1999. Strain 24eomechanics measurements in undrained plane-strain biaxial tests on Hostun RF sand. Mechanics of Cohesive-Frictional Materials, 4(4):419–441.
40. Mooney, M.A., Finno, R.J., and Viggiani, G.1998. A unique critical state for sand? Journal of Geotechnical and Geoenvironmental Engineering, ASCE, **124**(11):1100–1108.
41. NGF.1974. Guidelines by the Norwegian Geotechnical Forum on presentation of the geotechnical investigation". Norwegian Geotechnical Forum, Oslo, Norway.
42. Nordal, S., Alen, C., Emdal, A., Jendeby, L., Lyche, E. and Madshus, C. 2009. Skredet i Kattmarkvegen i Namsos 13. Mars 2009. A report to the transportation Ministry of Norway, ISBN 978-82-92506-71-4 (paper version) ISBN 978-82-92506-72-1 (electronic version).
43. Rhee, Y. 1991. Experimental evaluation of strain- softening behavior of natural and reconstituted samples of two over consolidated clays. Proceedings of the International Symposium on Hard Soils and Soft Rocks, Athens, Greece, 1, pp. 769-778.
44. Roger V, Desrues J, Viggiani G.1998. Experiments on strain 24eomechanics in dense sand under isochoric conditions. In Localization and Bifurcation Theory for Soils and Rocks, Adachi T, Oka F, Yashima A (eds). Balkema: Rotterdam, pp. 239–248.
45. Rosenqvist, I. 1953. Consideration on the sensitivity of Norwegian quick clay. Geotechnique, **5(**1): 95-200.
46. Saada, A. S., Bianchini, G. F., and Liang, L. 1994. Cracks, bifurcation and shear bands propagation in saturated clays. Geotechnique, **44**(1):35-64.
47. Sandven, R. 1990. Strength and deformation properties of fine grained soils obtained from piexocone tests. PhD Thesis, NTNU, Norway
48. Scavia, C., Viggiani, G., Castelli, M., and Desrues J. 1997. An experimental and numerical study of shear fracture propagation in rock. Deformation and Progressive Failure in Geomechanics, Proceedings of IS-Nagoya'97, A. Asaoka, T. Adachi and F. Oka (eds.), Pergamon, pp. 175-180.
49. Shuttle, D. A., and Smith, I. M. 1990. Localization in the presence of excess pwp. Computers and Geotechnics, 9(1), 87-89.
50. Skempton, A.W. and Northey, R.D. 1952. Sensitivity of Clays," Geotechnique, **3**(1): 40-51.
51. Teunissen, J. 2008. Shear Band Analysis in the Biaxial Test. International Journal of Geomechanics, **8**(5): 311–321.

52. Thakur, V. 2011. Numerically observed shear bands in quick clays.” International Journal of Geomechanics and Geoengineering, **6**(2):131-146.
53. Thakur, V. and Degago S.A. 2014. Quickness test approach for assessment of flow slide potentials. International Geotechnical Engineering Journal of the SEAGS & AGSSEA, 45(1): 85-94.
54. Thakur, V. and Degago,S. A.2012. Quickness of sensitive clays. Géotechnique Letters **2**(3): 87–95.
55. Thakur, V. and Degago,S. A.2013. Disintegration energy of sensitive clays. Géotechnique Letters **3**(1): 21–25.
56. Thakur, V. et al. (2014). Characterization of post-failure movements of landslides in soft sensitive clays. Natural Hazards book: Advances in Natural and Technological Hazards Research, 36, pp. 91-103.
57. Thakur, V., Grimstad, G., and Nordal, S. 2006. Instability in quick clays. Proceedings of the Engineering Conference International Series: Geohazards, Lillehammer, Norway, P7, http://services.bepress.com/eci/geohazards/43Thakur 2006
58. Thakur, V., Nordal, S., Jostad, H. P., and Andresen, L. 2005. Study on pwp dissipation during shear banding in sensitive clays. 11th International conference on computer methods and advances in geomechaincs, IACMAG, Turino, Italy, 4,pp. 289-296.
59. Thakur, V., Nordal, S., Stijacic, A., Jostad, H.P., Andresen, L.2008. Numerical modelling of orientation of partly drained shear band. *In* Proceedings of 12th international conference of international association for computer methods and advances in 25eomechanics, Goa, pp. 1132–1139
60. Thakur V, Degago S A, Oset F, Dolva B K and Aabøe R (2013) A new approach to assess the potential for flow slide in sensitive clays. Une nouvelle approche pour évaluer le potentiel de Coulée dans les argiles sensibles. International conference on soil mechanics and geotechnical engineering, ISSMGE, Paris, France, pp 2265-2269.
61. Topolnicki, M., Gudehus, G., and Mazurkiewicz, B. K. 1990. Observed stress-strain behavior of remoulded saturated clay under plane strain conditions. Geotechnique, **40**(2): 155-187.
62. Vardoulakis I, Goldscheider M.1981. Biaxial apparatus for testing shear bands in soils. Proceedings, 10th ICSMFE, Stockholm. Balkema: Rotterdam, 4/61,pp. 819–824.
63. Vardoulakis I.1988. Theoretical and experimental bounds for shear-band bifurcation strain in biaxial tests on dry sand. Research Mechanica, **23**:239–259.
64. Vardoulakis, I. G. and Goldscheider, M. 1981. Biaxial apparatus for testing shear bands in soils, Proc. 10th Int. conf. on oil Mechanics and Foundation Engineering, Stockholm, 4, pp. 819-824.
65. Viggiani, G., Finno, R. J., and Harris, W. W. 1994. Experimental observations of strain localization in plane strain compression of a stiff clay. In: Localization and Bifurcation Theory for Soils and Rocks, R. Chambon, J.Desrues & I. Vardoulakis editors, Balkema, pp.189-198.
66. Viggiani, G., Küntz, M., and Desrues J. 2001. An experimental investigation of the relationship between grain size distribution and shear banding in granular materials.” Continuous and Discontinuous Modeling of Cohesive Frictional Materials, P.A. Vermeer et al. (Eds.), Springer, pp. 111-127.
67. Yoshida, T., Tatsuoka, F., Kamegai, Y., Siddiquee, M.S.A., Park, C.S.1994.. Shear banding in sands observed in plane strain compression. Localisation and Bifurcation Theory for Soils and Rocks, Chambon R, Desrues J, Vardoulakis I (eds). Balkema: Rotterdam, pp. 165–179.

68. Yuan, J., Zhang, Q., Li, B., and Zhao, X. 2013. Experimental analysis of shear band formation in plane strain ests on Shanghai silty clay. Bull Eng Geol Environ, **72**: 107–114.
69. Zhou, H., and Randolph, M. F. 2007. Computational Techniques and Shear Band Development for Cylindrical and Spherical Penetrometers in Strain-Softening Clay." International Journal of Geomechanics, **7**(4): 287-295.

Table 1 A summary of different sensitivity scales proposed in the literature.

Sensitivity (S_t)	Classifications
1	Non sensitive
1–8	LS
8–16	HS/ES/SQ
16–32 (30)	Q/MQ
>32	Q

L: low; M: medium; H: high; E: extra; S: sensitive; Q: quick

Table 2. Summary of the Physical and Mechanical Properties of Tiller Quick Clay

Soil Parameters	
Unit weight, γ, [kN/m^3]	18.4–18.7
Natural water content, w, [%]	33–40
Liquid limit, w_L, [%]	24–26
Plastic limit, w_P, [%]	18
Plasticity index, I_p, [%]	6–8
Liquidity index, I_L, [-]	1.5–1.8
Undrained shear strength, c_u, [kPa]	18–25
Effective frictional angle, φ, [degrees]	26.5
Effective cohesion, c, [kPa]	6
Remolded undrained shear strength, c_{ur}, [kPa]	0.1–0.3
Sensitivity, S_t, [-]	83–180
Over consolidation ratio [-]	1.3-1.6

Table 3. Testing Program

Tests	Rate of axial shortening [mm/min]	In-situ effective vertical stress σ_{zo}' [kPa]	Selected confining pressure* [kPa] $= K_o' \cdot \sigma_{zo}'$	Probe locations^
T1	0.06	120	70	Left and Right (LP, RP)
T2	0.06	100	60	Central and Bottom (CP,BP)
T3	0.06	100	65	Central and Bottom (CP,BP)
T4	0.06	100	63	Central and Bottom (CP,BP)
T5	0.006	100	60	Central and Bottom (CP,BP)
T6	0.006	120	70	Central and Top (CP,TP)

** $K_o' = 0.6$*

^ CP, BP and TP, were always placed on the left side of the specimen

Figure captions

Figure 1. An illustration of the effect of sample disturbance on the results from consolidated undrained triaxial compression (CUC) test and constant rate of strain odometer on Tiller quick clays sampled using a 54 mm-diameter cylinder, and a 160 mm-diameter mini Sherbrook block sampler developed by Emdal et al. (2016). The CUC tests were done at 1.2%/hr strain rate and the CRS tests were done at 6.0 %/hr. The properties of the tested materials are given in Table 2. Here, M is the odometer modulus, ε_v is the volumetric strain, p' is the mean effective stress, q is the deviator stress.

Figure 2. Excess pwp may develop and then dissipate during the formation and propagation of shear bands in slopes and laboratory samples of quick clay. The shear stress and shear strain patterns for two soil elements A and B are shown in the figure. Element A is located inside the shear band whereas element B is outside the shear band. The element A is already subjected to strain softening whereas the element B is yet to reach to the peak shear stress.

Figure 3: The plane strain apparatus

Figure 4. Specimen preparation for the tests: (1) Mold in the split form: outer and inner shells; (2) Assembled mold; (3) Membrane placed on the outer shell and lateral supports mounted to support the top plate; (4) Inner shell holding a specimen placed inside the outer shell; (5) Shells can be removed together, leaving the specimen inside the membrane.

Figure 5. Left: Quick clay specimen with pore water pressure transducers and lateral supports; middle: Quick clay specimen mounted in the plane-strain apparatus; Right: Schematic of the specimen size and the axis direction adopted in this study.

Figure 6. Shear stress (t) and nominal axial strain (ε) plots for the tested specimen.

Figure 7. DIC results (total and incremental shear strain field) for the T2 test. (a): Shear stress deformation pattern the location of the images, P0 to P8, along the curve (b): Normalized pore water pressure non-uniformity versus deformation behavior and the location of the images, P0 to P7, along the curve. (c): The total shear strain distribution on the sample surface computed using the DIC technique. (d): The incremental shear strain distribution on the sample surface computed using the DIC technique. *[Note: the colored images can be found in the electronic version of this paper]*.

Figure 8. DIC results (total and incremental shear strain field) for the T5 test. (a): Shear stress deformation pattern the location of the images, P0 to P8, along the curve (b): pore water pressure non-uniformity versus deformation behavior and the location of the images, P0 to P7, along the curve. (c): The total shear strain distribution on the sample surface computed using the DIC technique. (d): The incremental shear strain distribution on the sample surface computed using the DIC technique. *[Note: the colored images can be found in the electronic version of this paper]*.

Figure 9. DIC results (total and incremental shear strain field) for the T6 test. (a): Shear stress deformation pattern the location of the images, P0 to P8, along the curve (b): pore water pressure non-uniformity versus deformation behavior and the location of the images, P0 to P7, along the curve. (c): The total shear strain distribution on the sample surface computed using the DIC technique. (d): The incremental shear strain distribution on the sample surface computed using the DIC technique. *[Note: the colored images can be found in the electronic version of this paper]*.

Figure 10. Effective stress paths obtained for the plane strain tests. In this figure, *s'* represents the mean effective stress $((\sigma_z{}' + \sigma_x{}')/2)$, t denotes the shear stress $(\sigma_z{}' - \sigma_x{}')/2$, and σ' are the effective stresses; the subscripts z and x stand for the axial and horizontal direction in the plane of deformation. The dotted line refers to a failure line corresponding to c = 6 kPa and φ = 26.5^{o}. The selected c and φ values are typical for Norwegian quick clays.

Figure 11. Measured pwp (p_w) at the probe locations vs nominal axial strain (ε) plots for the plane strain tests. The location of the probes on sample is shown on the plots. Here LP, RP, CP, BP, and TP refers to left probe, right probe, central probe, bottom probe and top probe respectively. Here, $\sigma_{x0}{}'$ is the effective cell pressured as given in Table 3 and H is the sample height which is equal to 120 mm.

Figure 12. Pore water pressure non-uniformities observed for quick clay (this study) and a comparison with Shanghai silty clay reported by Yuan et al. (2013)

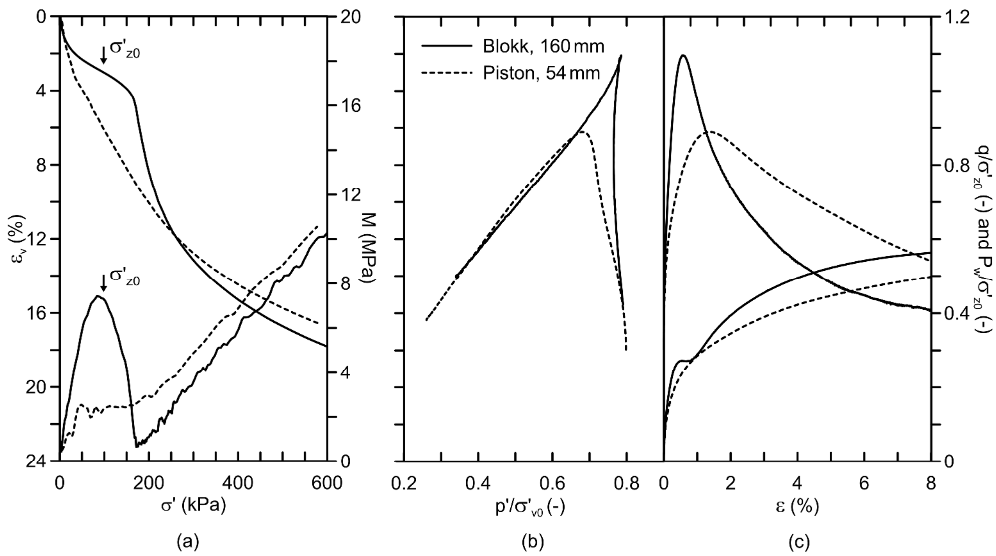

Figure 1. An illustration of the effect of sample disturbance on the results from consolidated undrained triaxial compression (CUC) test and constant rate of strain odometer on Tiller quick clays sampled using a 54 mm-diameter cylinder, and a 160 mm-diameter mini Sherbrook block sampler developed by Emdal et al. (2016). The CUC tests were done at 1.2%/hr strain rate and the CRS tests were done at 6.0 %/hr. The properties of the tested materials are given in Table 2. Here, εv is the volumetric strain P' is the mean effective stress, q is the diviator stress, M is the oedometer modulus,

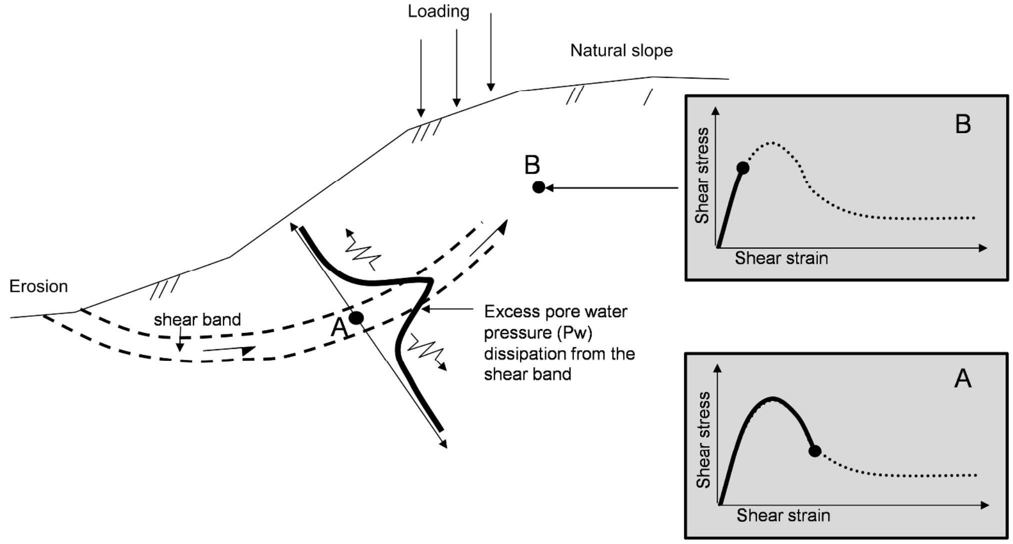

Figure 2. Excess pore water pressure may develop and then dissipate during the formation and propagation of shear bands in slopes and laboratory samples of quick clay. The shear stress and shear strain patterns for two soil elements A and B are shown in the figure. Element A is located inside the shear band whereas element B is outside the shear band. The element A is already subjected to strain softening whereas the element B is yet to reach to the peak shear stress.

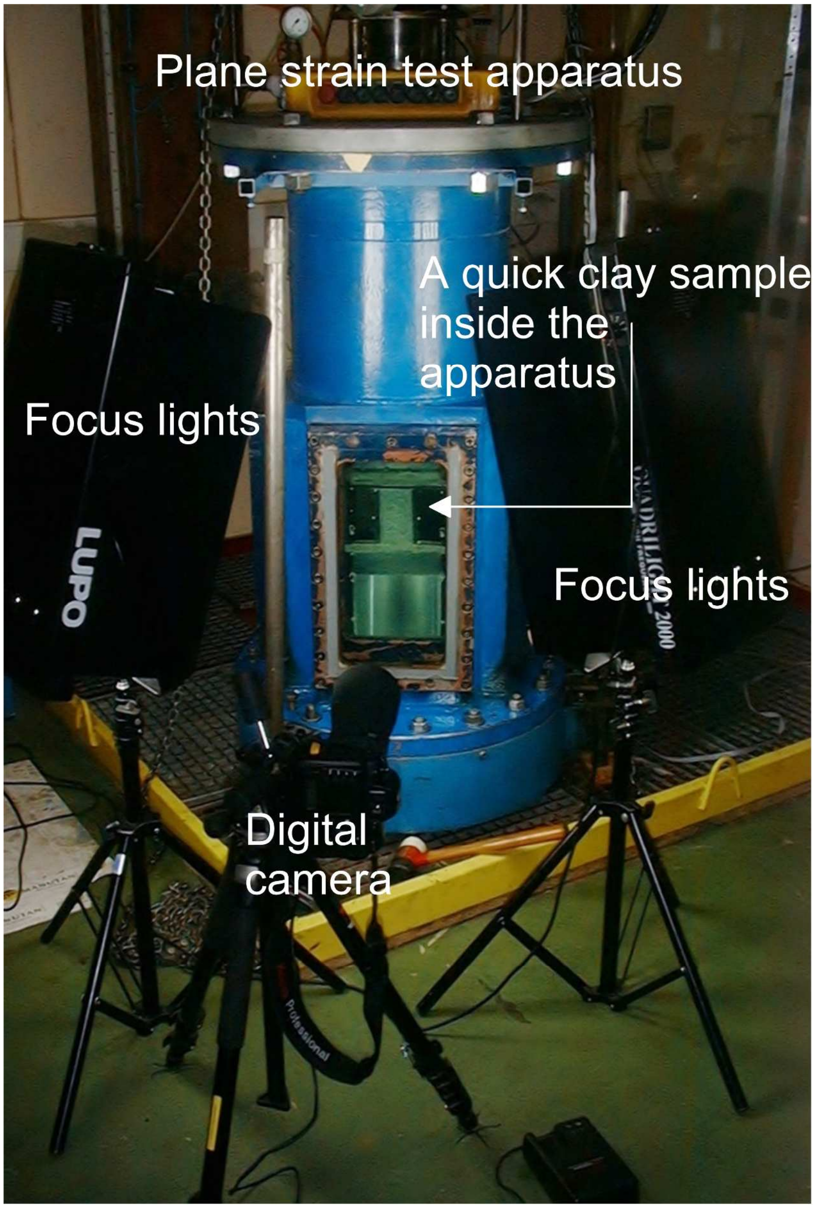

Figure 3: The plane strain apparatus

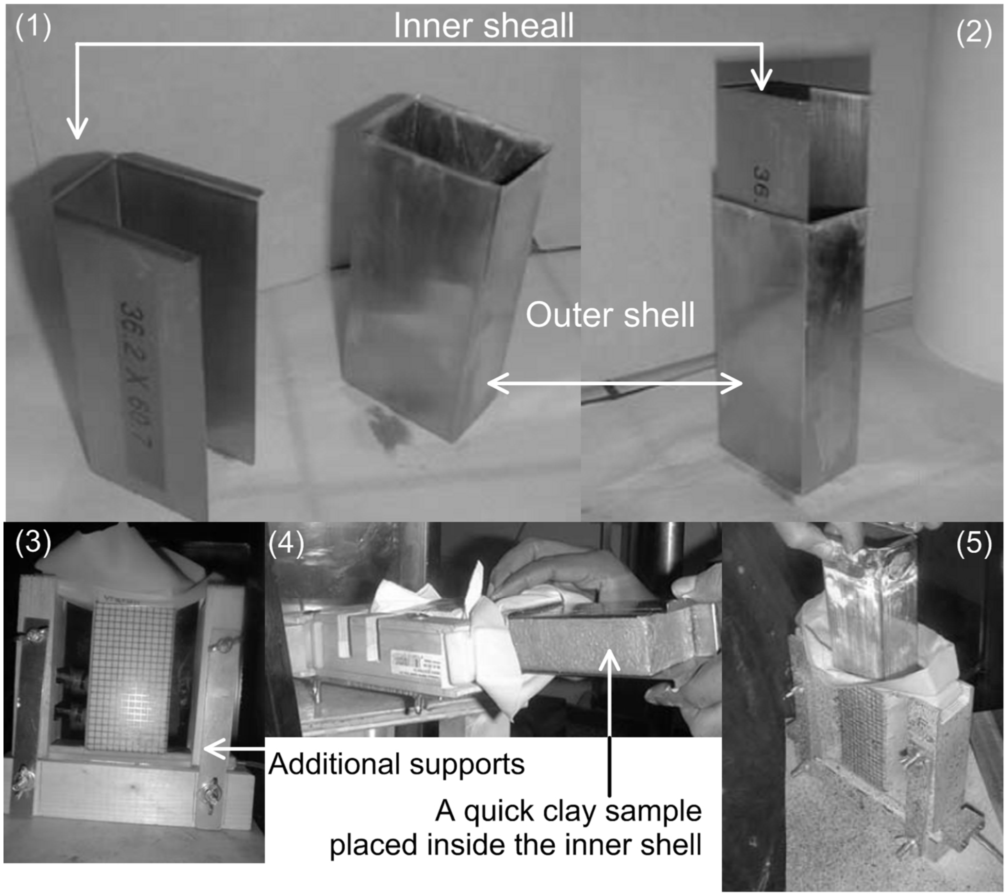

Figure 4. Specimen preparation for the tests: (1) Mold in the split form: outer and inner shells; (2) Assembled mold; (3) Membrane placed on the outer shell and lateral supports mounted to support the top plate; (4) Inner shell holding a specimen placed inside the outer shell; (5) Shells can be removed together, leaving the specimen inside the membrane.

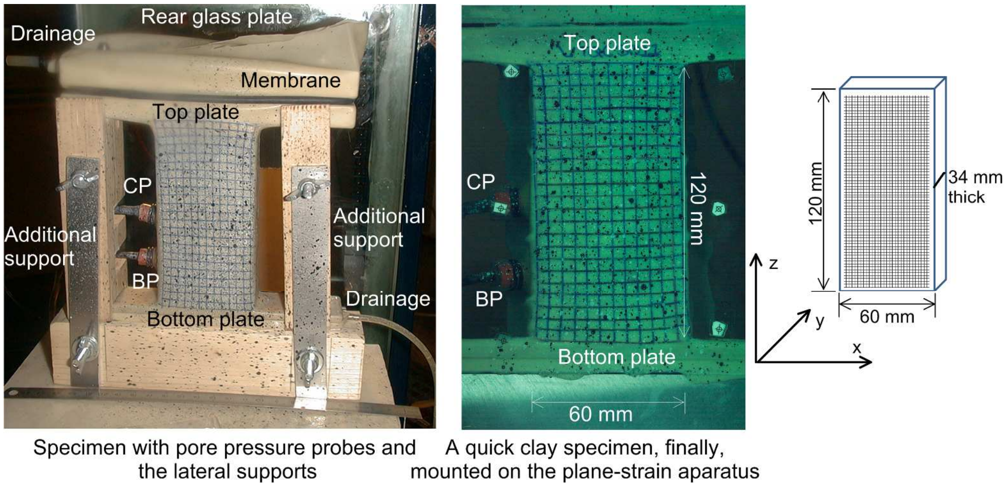

Figure 5. Left: Quick clay specimen with pore water pressure transducers and lateral supports; middle: Quick clay specimen mounted in the plane-strain apparatus; Right: Schematic of the specimen. The locations of the pore water pressure probes on the samples are shown, CP is the central probe and BP is the bottom probe.

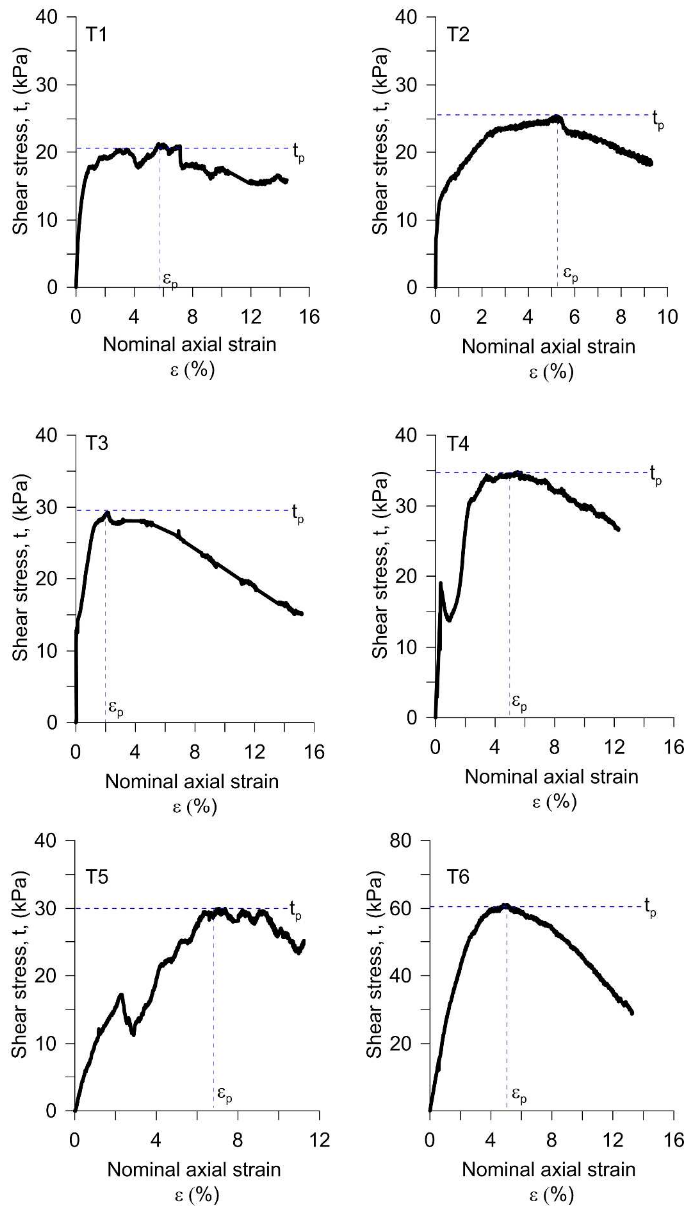

Figure 6. Shear stress (t) and nominal axial strain(ε) plots for the tested specimen

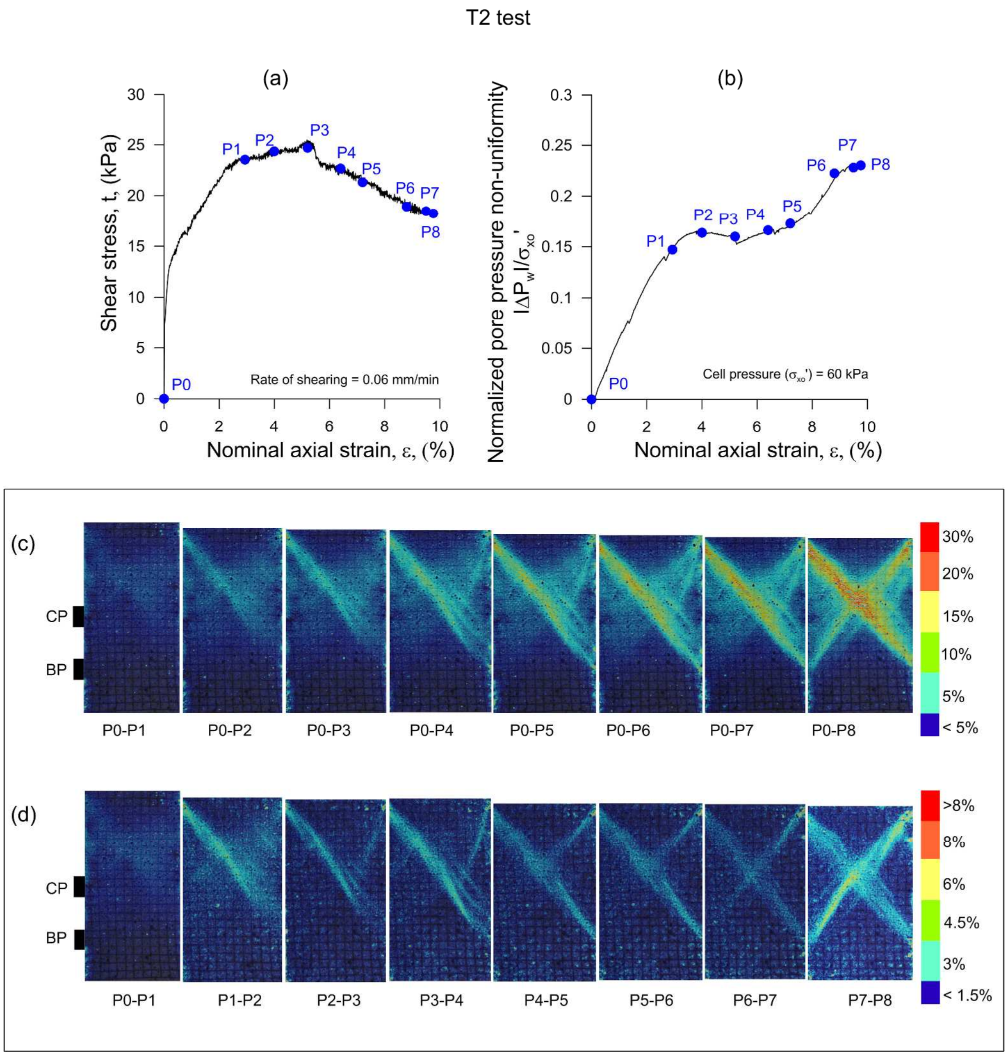

Figure 7. DIC results for the T2 test. (a): Shear stress versus relative deformation (nominal or globally measured strain). The positions P0 to P8 show where images are taken. (b): Normalized pore water pressure difference (CP – BP) versus relative deformation, (reset to zero difference at the end of consolidation). (c): The total shear strain distribution on the sample surface computed using the DIC technique. (d): The incremental shear strain distribution on the sample surface computed using the DIC technique. [Note: the colored images can be found in the electronic version of this paper].

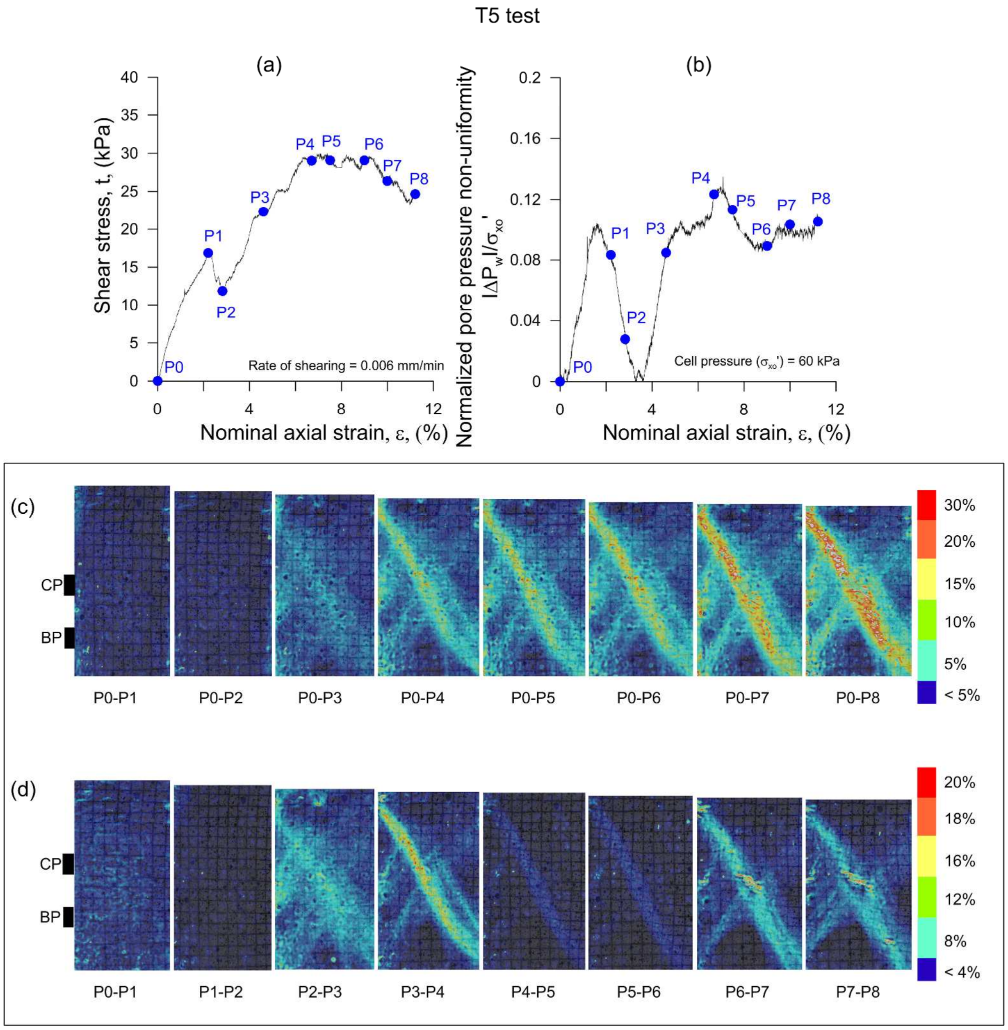

Figure 8. DIC results for the T5 test. (a): Shear stress versus relative deformation (nominal or globally measured strain). The positions P0 to P8 show where images are taken. (b): Normalized pore water pressure difference (CP – BP) versus relative deformation, (reset to zero difference at the end of consolidation). (c): The total shear strain distribution on the sample surface computed using the DIC technique. (d): The incremental shear strain distribution on the sample surface computed using the DIC technique. [Note: the colored images can be found in the electronic version of this paper].

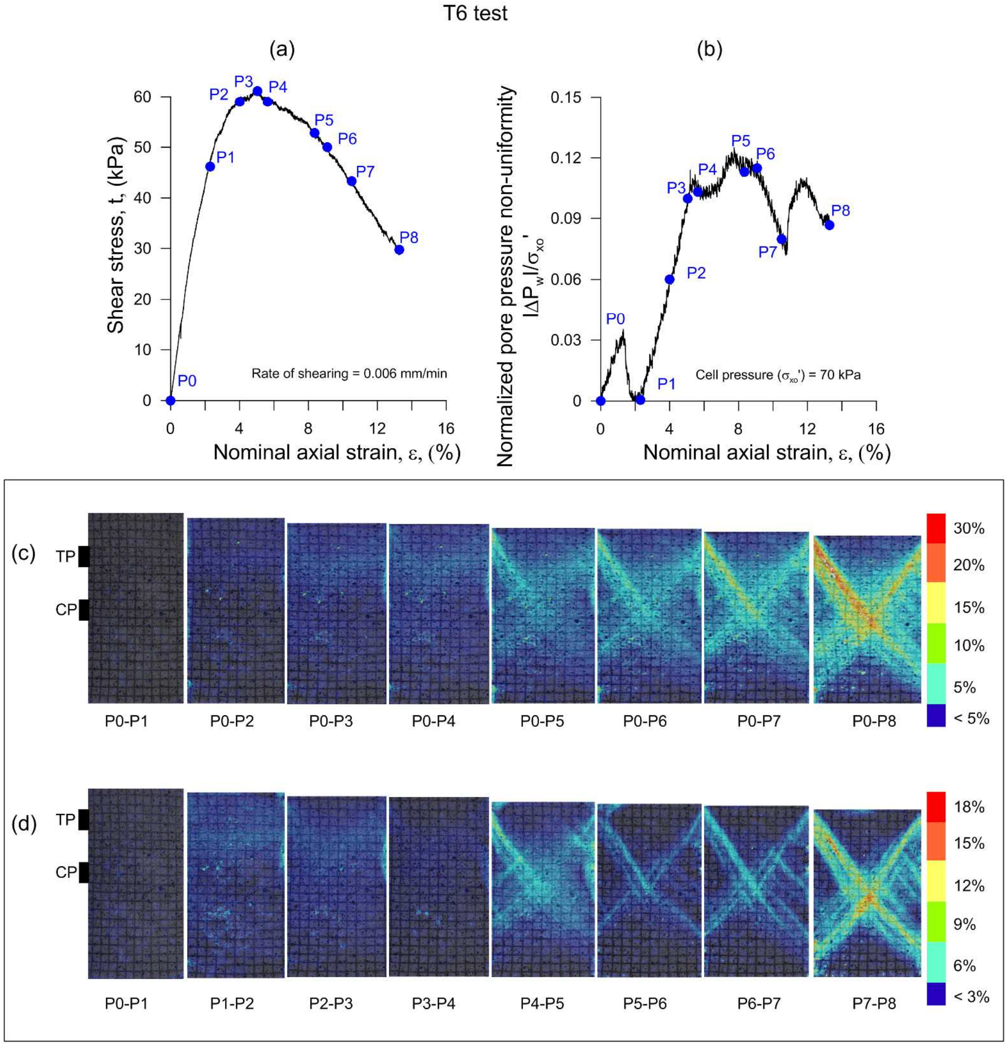

Figure 9. DIC results for the T6 test. (a): Shear stress versus relative deformation (nominal or globally measured strain). The positions P0 to P8 show where images are taken. (b): Normalized pore water pressure difference (TP – CP) versus relative deformation, (reset to zero difference at the end of consolidation). (c): The total shear strain distribution on the sample surface computed using the DIC technique. (d): The incremental shear strain distribution on the sample surface computed using the DIC technique. [Note: the colored images can be found in the electronic version of this paper].

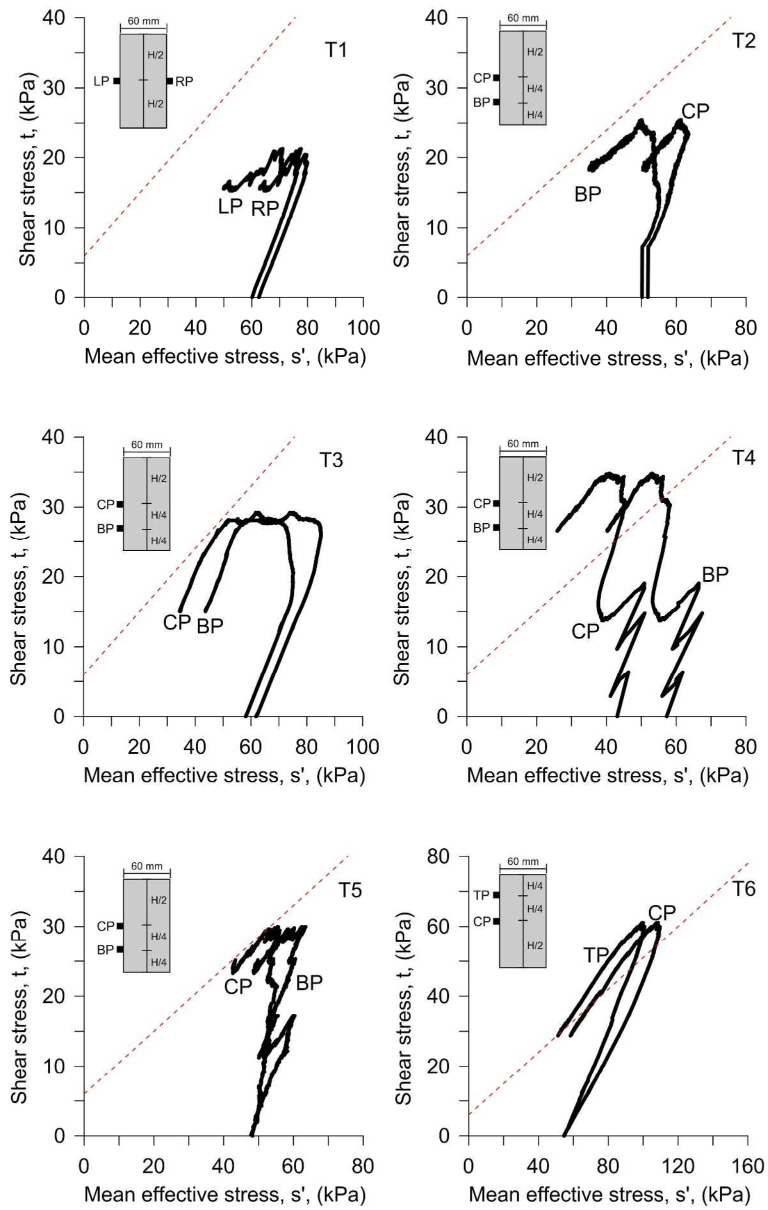

Figure 10. Effective stress paths obtained for the plane strain tests. In this figure, s' represents the mean effective stress ((σz'+σx')/2), t denotes the shear stress (σz'- σx')/2, and σ' are the effective stresses; the subscripts z and x stand for the axial and horizontal direction in the plane of deformation. The dotted line refers to a failure line corresponding to c = 6 kPa and φ = 26.5o. The selected c and φ values are typical for quick clays for this site.

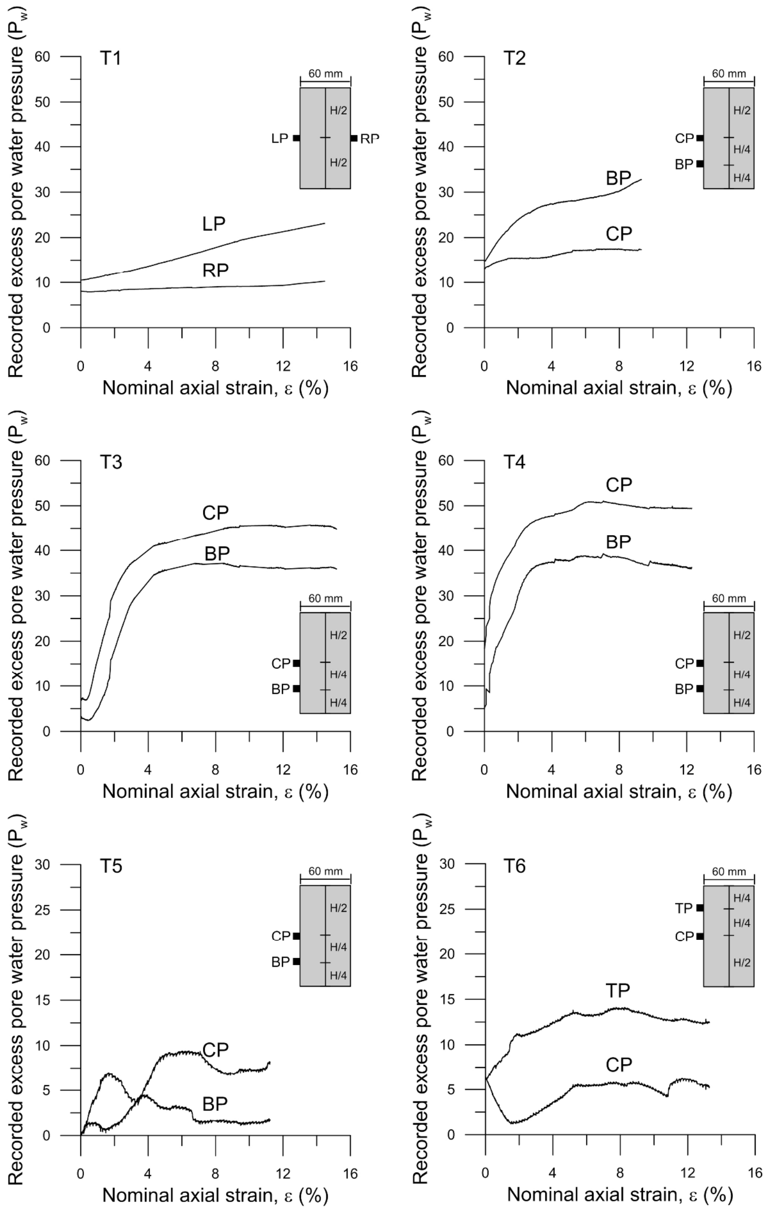

Figure 11 Measured pore water pressure at the probe locations vs relative deformation (ε) for the plane strain tests. The locations of the probes on the samples are shown. LP, RP, CP, BP, and TP refers to left probe, right probe, central probe, bottom probe and top probe respectively. Here, σx0' is the effective cell pressured as given in Table 3 and H is the sample height which is equal to 120 mm. The graphs focus on differences in pore water pressure development between the probes and is therefore set to zero at the beginning of the shear phase.

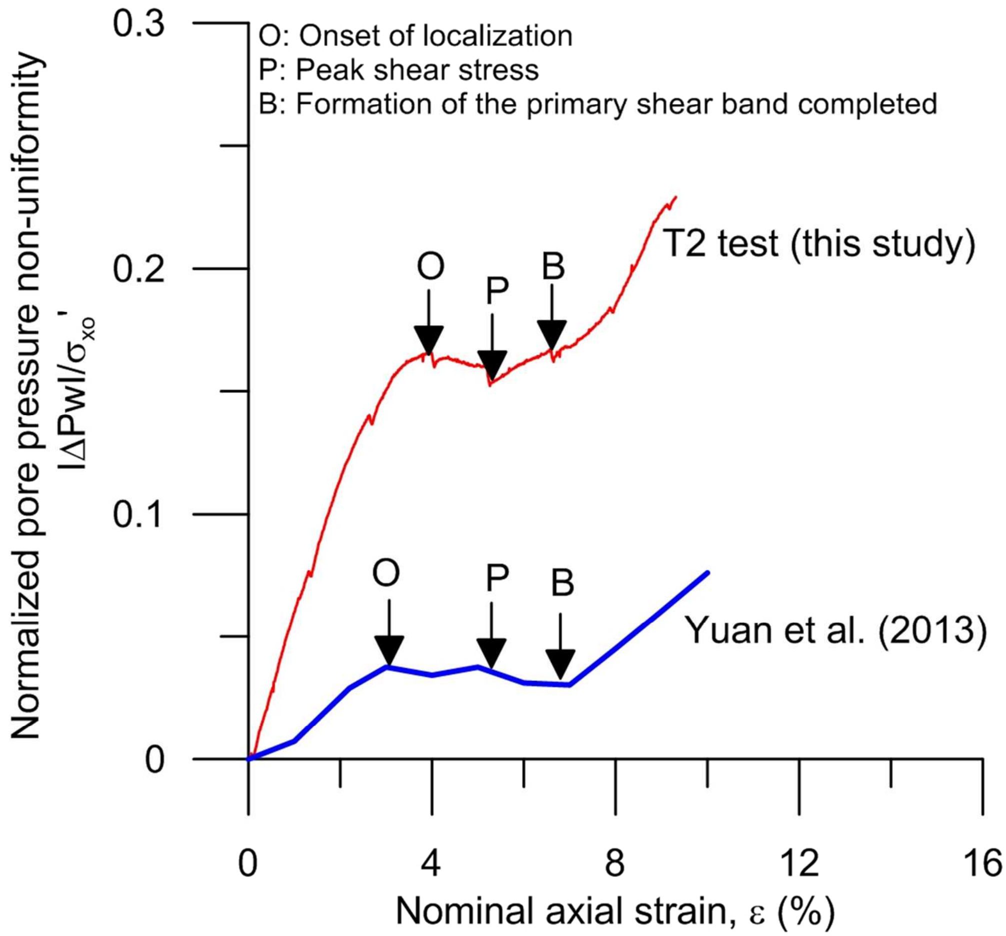

Figure 12. Pore pressure non-uniformities observed for quick clay (this study) and a comparison with Shanghai silty clay reported by Yuan et al. (2013)